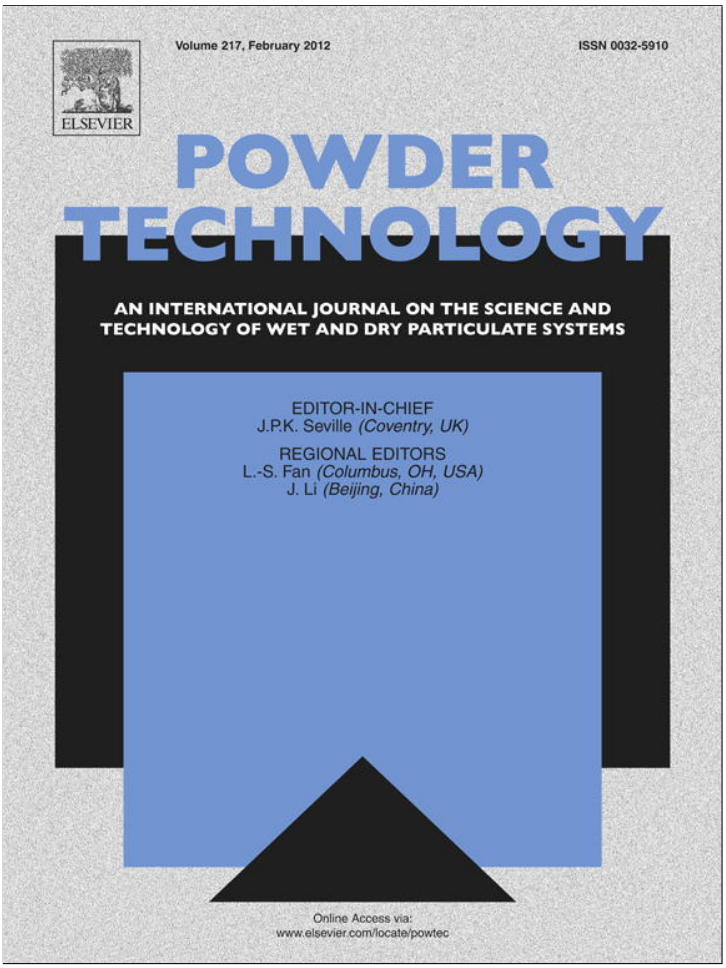

Powder Technology 217 (2012) 330–339

Contents lists available at SciVerse ScienceDirect

Powder Technology

journal homepage: www.elsevier.com/locate/powtec

Investigation of the catalytic activity of nano-sized CuO, Co_3O_4 and $CuCo_2O_4$ powders on thermal decomposition of ammonium perchlorate

Ebrahim Alizadeh-Gheshlaghi [a,b,*], Behrouz Shaabani [a,b], Ali Khodayari [c], Yashar Azizian-Kalandaragh [d], Rahmatollah Rahimi [e]

[a] Department of Chemistry, Islamic Azad University, Ardabil Branch, Ardabil, Iran
[b] Department of Inorganic Chemistry, Faculty of Chemistry, Tabriz University, Tabriz, Iran
[c] Department of Chemistry, University of Mohaghegh Ardabili, P.O. Box 179, Ardabil, Iran
[d] Department of Physics, University of Mohaghegh Ardabili, P.O. Box 179, Ardabil, Iran
[e] Department of Chemistry, Iran University of Science and Technology, Narmak, Tehran 16846-13114, Iran

ARTICLE INFO

Article history:
Received 2 July 2011
Received in revised form 21 October 2011
Accepted 23 October 2011
Available online 29 October 2011

Keywords:
Metal oxide
Semiconductors
Catalysis
Ammonium perchlorate
DSC

ABSTRACT

In the present work, nano-sized CuO, Co_3O_4 and $CuCo_2O_4$ powders were prepared via different methods such as co-precipitation, thermal decomposition of oxalate precursor and sol–gel and their catalytic activities towards thermal decomposition of ammonium perchlorate were investigated using DSC technique. $CuCo_2O_4$ showed better catalytic activity than others and the thermal decomposition temperature of ammonium perchlorate shift downward about 103 °C. The catalytic mechanism was also briefly discussed. TG-DSC, FT-IR, XRD, SEM, TEM and BET techniques were applied for studying of thermal behavior, examination of catalytic activity, spectroscopic, structural, morphological characterization and determination of specific surface area of synthesized powders, respectively.

1. Introduction

Inorganic 3d-transition metal oxides have attracted tremendous attention due to their remarkable catalytic, magnetic, optical, electrical properties and potential application in many fields of engineering and science [1–3]. Nano-sized Co_3O_4 and CuO are important inorganic p-type semiconductors with direct optical band gaps at 3.95–2.13 eV [4] and 1.4 eV [5] respectively. Cobalt and copper oxide powders have a wide range of applications in various fields of industry including anode materials for rechargeable Li-ion batteries [6], gas sensors, solid-state sensors, ceramic pigments, heterogeneous catalysts, rotatable magnets, electrochromic devices, magnetic materials and in energy storage [7–11]. Much efforts have been made to prepare Co_3O_4 and CuO nanoparticles, including pulsed laser deposition [12], sol–gel route [13], chemical spray pyrolysis [14], gel hydrothermal oxidation, ionic liquid-assisted [15], hydrothermal [16], polymeric citrate [17,18], and the reverse micellar method [19].

Complex oxides (containing two or more types of cations) with spinel structure are of intense interests in material research because of their remarkable optical, electrical, magnetic, catalytic properties and widespread applications in science and engineering. Among these, spinel cobaltites (MCo_2O_4; M=Co, Cu, Mn, Ni, Zn, Mg, etc.) have recently drawn considerable attention by virtue of their superior physicochemical properties and tremendous potential for many technological applications, ranging from catalysts and sensors to electrode materials and electrochromic devices [20].

In this work, the two investigated systems are the spinel cobaltite with the initial formula MCo_2O_4 (M=Co(II), Cu(II)). Their normal and inverse spinel structures with two different crystallographic sublattices for the cations can be represented by a general formulas $A[B]_2O_4$ and $B[AB]O_4$ respectively; where elements A and B denote divalent and trivalent metallic cations, respectively, and cations inside the parenthesis are octahedrally and those outside are tetrahedrally coordinated with oxygen ions [21]. In $Co^{2+}[Co^{3+}]_2O_4^{2-}$ (Co_3O_4—normal spinel), the Co^{3+} cations complete the B sites and the Co^{2+} cations occupy the A sites [22,23]. S. Angelov and et al. found that in the case of $Cu_xCo_{3-x}O_4$ when $x>0.2$ a transition occurred from a normal to an inverse spinel [24]. In $Cu^{2+}[Co^{3+}]_2O_4^{2-}$ ($CuCo_2O_4$-inverse spinel) the Co^{3+} cations complete the A sites and half of B sites, and Cu^{2+} cations occupy B sites [25] and is a typical John–Teller ion.

Copper cobaltite inverse spinel with the general formula $Cu_xCo_{3-x}O_4$ (here $x=1$) is well known for the catalytic activity toward the oxidation of CO to CO_2, alcohol synthesis, automobile pollution control and oxygen evolution [26–30]. Cubic $CuCo_2O_4$ inverse spinel crystals with various structural/morphological characteristics (i.e., particle size, shape, stoichiometry and cation distribution) have been prepared by diverse synthetic

* Corresponding author at: Azad University of Ardabil, Iran. Tel: +98 411 3393144; fax: +98 411 3340191.
E-mail address: e.a.ahari@gmail.com (E. Alizadeh-Gheshlaghi).

0032-5910/$ – see front matter © 2011 Elsevier B.V. All rights reserved.
doi:10.1016/j.powtec.2011.10.045

routes including nitrate decomposition [3,27], urea combustion [31], co-precipitation [32–34,57], sol–gel [35,57], hydrothermal [36], aerosolpyrolysis [37], anodic electrodeposition [38] and so forth.

Ammonium perchlorate (AP) is the main composition in many propellants. The application of superfine AP can improve the performance of propellants to some extent. However, the preparation of superfine AP is very dangerous and difficult, because the material of AP is a kind of strong oxidant [39]. The activation energy, reaction rate and pyrolysis temperature of the thermal decomposition of AP are related to the properties of solid propellants, especially the combustion rate. The lower the pyrolysis temperature, the shorter the delay time of propellant ignition, and the higher the combustion rate [40]. The performances of propellants can be improved further more by adding a small amount of catalyst in superfine AP.

The catalytic applications of some transition metals and their oxides for the thermal decomposition of AP have been widely studied [41–44]. To the best of our knowledge, there is no report on the comparative investigations of catalytic behaviors of Co_3O_4, CuO and $CuCo_2O_4$ on the thermal decomposition of AP. Central in this study is synthesizing maintained nano metal oxides with different methods and investigation of their catalytic activity on the thermal decomposition of Ammonium perchlorate.

2. Experimental details

2.1. Materials

All the AR-chemical reagents purchased from Merck and Sigma-Aldrich and used as received without further purification. In all synthesis methods, metal and M are Co, Cu and (1Co + 2Cu).

2.2. Synthesis

2.2.1. Co-precipitation method

The co-precipitation process was carried out at 50 °C with 50 mL of 0.6 M metal nitrate solution added drop wise to 100 mL of 3.2 M NaOH solution; 100 mL of H_2O_2 (50 wt.%) was then introduced drop wise under constant stirring. The color of mixture changed to dark brown. In order to avoid the contamination of chloride ion, the H_2O_2 was used as an oxidizing agent instead of NaOCl [41]. The obtained precipitate was filtered, washed with deionized water and dried in an oven at 110 °C for 24 h. The dried precipitate was ground and calcined at 350 °C for 2 h.

2.2.2. Oxalate decomposition method

A 0.3 M solution of metal nitrate was prepared by dissolving in ethanol. The temperature was raised to 50 °C and after 30 min of continuous stirring, oxalic acid (OA) was rapidly added to the solution. The molar ratio M:OA was 1. The system was kept at 70 °C under reflux for 2 h and a precipitate was obtained; then the acetic acid and some of the ethanol were evaporated and the resulting viscous gel was dried at 80 °C overnight. The dried metal oxalate was ground and calcined at 350 °C for 2 h. For obtaining pure $CuCo_2O_4$ spinel phase instead of CuO/Co_3O_4 composite in this method, the obtained precipitate for synthesis of $CuCo_2O_4$ was ground and calcined at 850 °C for 2 h.

2.2.3. Sol–gel method

Metal nitrate and mixture of ethyl acetate and citric acid (0.5:0.5 M) was dissolved in 50 mL of ethanol separately and then mixed with the molar ratio of Ligand:M = 1. Cetyltrimethylammonium bromide (CTAB) was added to the above mixed solution so that the molar ratio of CTAB:M was 0.2. The resultant homogeneous solution was continuously stirred for 2 h and the temperature was increased to the boiling point of the solution. The system was refluxed for 16 h and then concentrated to about 1/3 of the initial volume. The residual solution was kept at 60 °C to evaporate ethanol until gelatin was completed. The gel was heat treated at 100 °C for 2 h and polymeric citrate-acetate precursor was gained. Finally, the synthesized precursor was ground to a fine powder and calcined in air at 400 °C for 2 h.

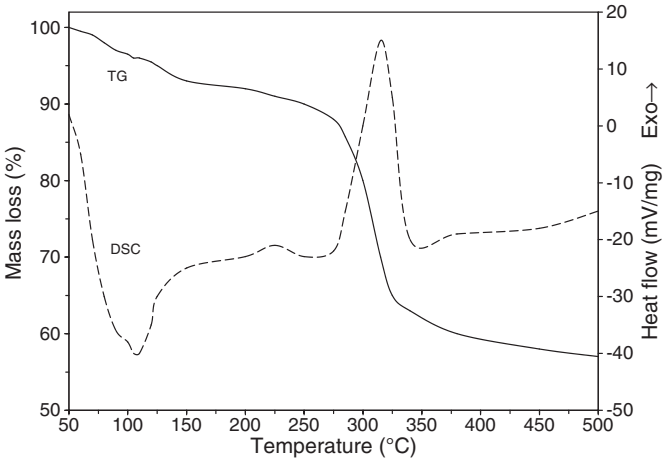

Fig. 1. TG-DSC curves of $Cu(OH)_2$ (co-precipitation method).

2.2.4. Catalytic activity tests

AP was selected as a target material for investigation of catalytic activity of these nano materials. Synthesized nano metal oxides powders via sol–gel method and AP were mixed in 3:97 mass ratios to prepare the samples for thermal analysis.

2.3. Characterization

X-ray Diffraction (XRD) patterns were recorded by a Bruker D8-Advance diffractometer using Cu Kα radiation (λ = 1.5406 Å). Fourier Transform Infrared (FT-IR) spectra were recorded on a Bruker-vertex70 spectrophotometer in KBr pellets. Surface morphology of product was characterized by using a LEO-1430.VP Scanning Electronic Microscopy (SEM) with an accelerating voltage of 15 kV. TEM images were prepared on a Philips EM208 transmission electron microscope operated at an accelerating voltage of 100 kV. The BET specific surface area of the synthesized nano-particles was determined by nitrogen adsorption at liquid nitrogen temperature on a Sibata SA-1100 surface area analyzer. The thermal decomposition processes of the samples were characterized by Differential Scanning Calorimetry (DSC) using Mettler Toledo DSC823E instrument was used at a heating rate of 20 °C/min in N_2 atmosphere with Al_2O_3 as reference.

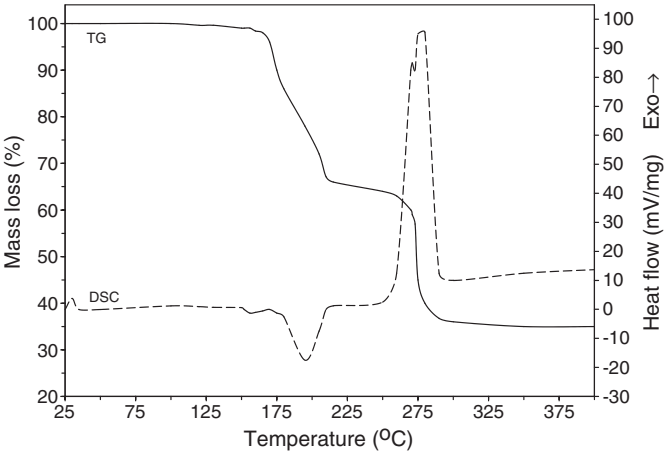

Fig. 2. TG-DSC curves of $Co(C_2O_4)$ (oxalate decomposition method).

3. Results and discussion

3.1. Characterization of structure and morphology

The thermal behavior of the precursors were investigated by TG-DSC method in temperature range 25–500 °C and their calcination temperatures were concluded from this method. Fig. 1 shows TG-DSC curves of copper hydroxide precipitate. According to the TG curve, this precursor has two weight loss steps. The first weight loss step occurs in temperature range of 100–180 °C attributed to water removing from precursor and second dominating weigh loss happens at about 280–320 °C, which is considered to the formation of final copper oxide. The DSC curve shows two endothermic and exothermic peaks at 110.24 and 318.54 °C that these peaks certify the obtained results from TG analysis respectively [45].

Fig. 2 shows thermal characteristics of cobalt oxalate. TG curve shows two weight loss steps in the temperature ranges of 175–220 and 260–310 °C. The first weight loss corresponds to the evaporation of crystallized water and formation of anhydrous cobalt oxalate in this stage. The value of weight loss in this step is about 17.75%, which is close to the theoretical value. The second weight loss can be attributed to the decomposition of $Co(C_2O_4)$ precursor and then formation of final cobalt oxide. The value of weight loss was found to be 41.2%, which corresponds to the loss of two moles carbon dioxide to form the cobalt oxide; the observed weight loss is close to the theoretical value (41%). The DSC curve shows two exothermic peaks at 197.02 and 275.14 °C, that these peaks certify the obtained dominant mass loss results from TG analysis.

TG-DSC curves of acetate-citrate precursor are shown in Fig. 3. Data extracted from these curves indicate that three-stage weight loss occurred by temperature rising. In TG curve, the first stage in the range of 50–180 °C is related to hydrated water and unreacted citric acid removing, which is specified by endothermic peak in DSC curve. The second weight loss in the range of 180–275 °C is associated to initial acetate–citrate complex and oxidation of organic materials which corresponding to endothermic peak around 210 °C. The last weight loss in temperature range of 320–400 °C is attributed to Cu – Co acetate–citrate complex decomposition with the formation of $CuCo_2O_4$ which corresponding to the DSC endothermic peak around 375 °C [46].

Room temperature powder X-ray diffraction patterns of synthesized products by sol–gel route were performed to identify the presence of crystalline phase in the samples that are shown in Fig. 4. Fig. 4-a shows the XRD pattern of obtained powder after calcining the copper citrate-acetate precursor in 400 °C for 2 h. All diffraction peaks in this pattern could be indexed to a pure monoclinic (Tenorite) crystalline (space group: C2/c [15]) of CuO with lattice parameters a = 4.68370 Å,

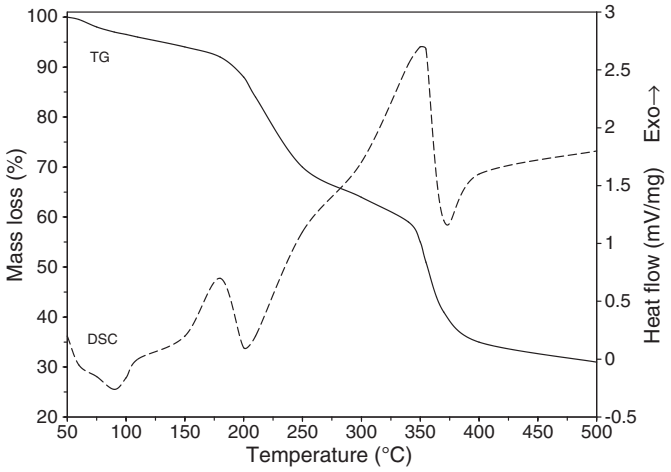

Fig. 3. TG-DSC curves of $CuCo_2$(acetate-citrate) (sol–gel method).

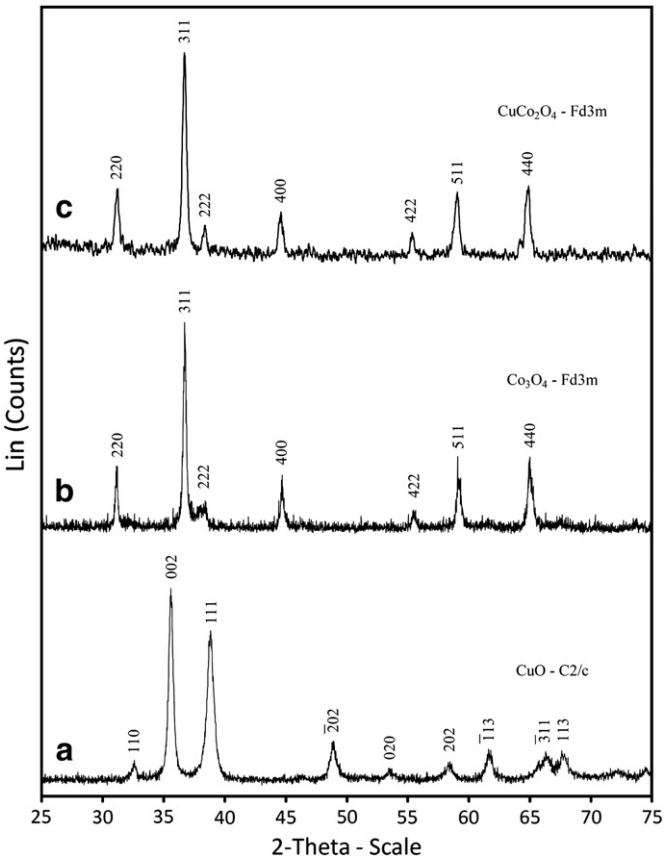

Fig. 4. XRD patterns of CuO (a), Co_3O_4 (b) and $CuCo_2O_4$ (c) prepared via sol–gel method.

b = 3.42260 Å, c = 5.12880 Å and β = 99.540 (ICDD card No. 72-0629). No obvious peaks of impurities were seen in this pattern such as Cu_2O, Cu, $Cu(NO_3)_2$, etc.

Fig. 4-b displays a typical XRD pattern of the nano crystalline Co_3O_4. All its diffraction peaks can be readily indexed to a pure face-centered cubic (fcc) structure (space group: Fd3m [227]) of Co_3O_4 normal spinel. The XRD pattern of $CuCo_2O_4$ is shown in Fig. 4-c. The diffraction peaks from this sample show a face-centered cubic structure (space group: Fd3m [227]) of $CuCo_2O_4$ inverse spinel. In two late XRD patterns, no diffraction peaks were seen arising from the possible impurity phases such as CuO, Cu_2O, CoO, CoO_2, Cu, Co, etc.

The unit cell's dimension of spinel structure was determined from d-spacing for the (220) and (311) plans by using the formula of a cubic lattice:

$$a_0 = d\left(h^2 + k^2 + 1^2\right)^{1/2}. \quad (1)$$

Here h, k and l are the Miller indices. Values of the unit cell's dimension 'a_0' were found to be 8.060 and 8.110 Å for the Co_3O_4 and $CuCo_2O_4$ respectively. However, a-value observed for Co_3O_4 is lower than its corresponding value in literature (a = 8.083 Å, ICDD card No. 42-1462) while for $CuCo_2O_4$ is higher than its corresponding value in literature (a = 8.105 Å, JCPDS card No. 37-0878). According to XRD data, a-value observed for Co_3O_4 is lower than $CuCo_2O_4$; thus, introduction of Cu increases the a-value. This increase can be attributed to the higher radii of Cu^{2+} in comparison with Co^{2+}. The ionic radii of the Cu^{2+} are 57 pm in the tetrahedral site and 73 pm in the octahedral site, while Co^{2+} are 58 pm in the tetrahedral site and 52.5 pm in the octahedral site. The ions radii difference of the two sites is 16 pm for the copper ions and 5.5 pm for the cobalt

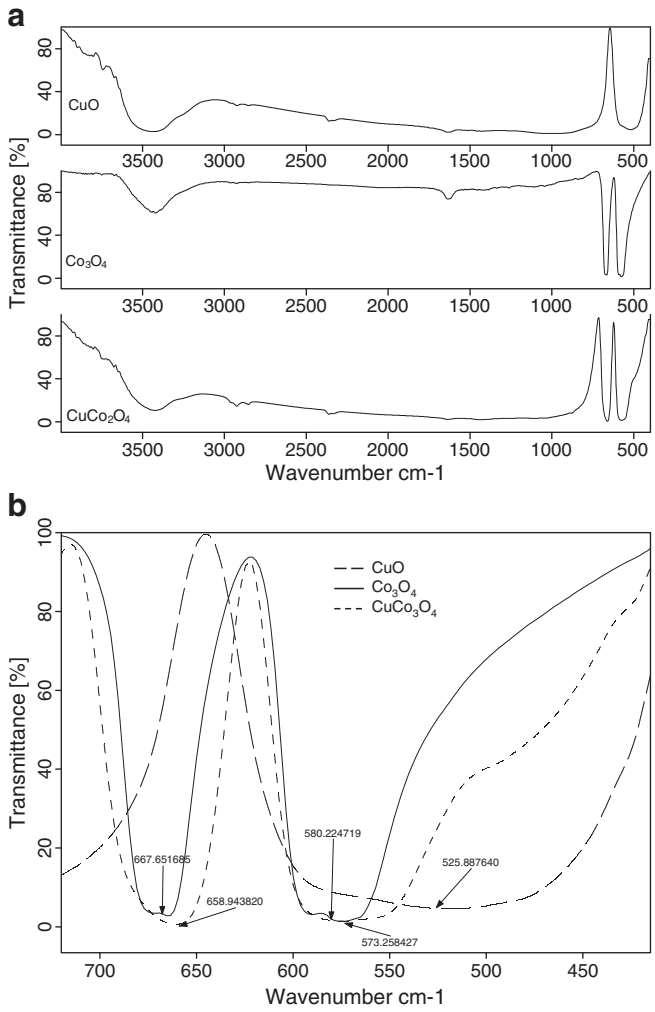

Fig. 5. FT-IR spectra of prepared nano-sized metal oxide powder via sol–gel method: mid-IR region (a) and zoomed region of 400–800 cm^{-1} (b).

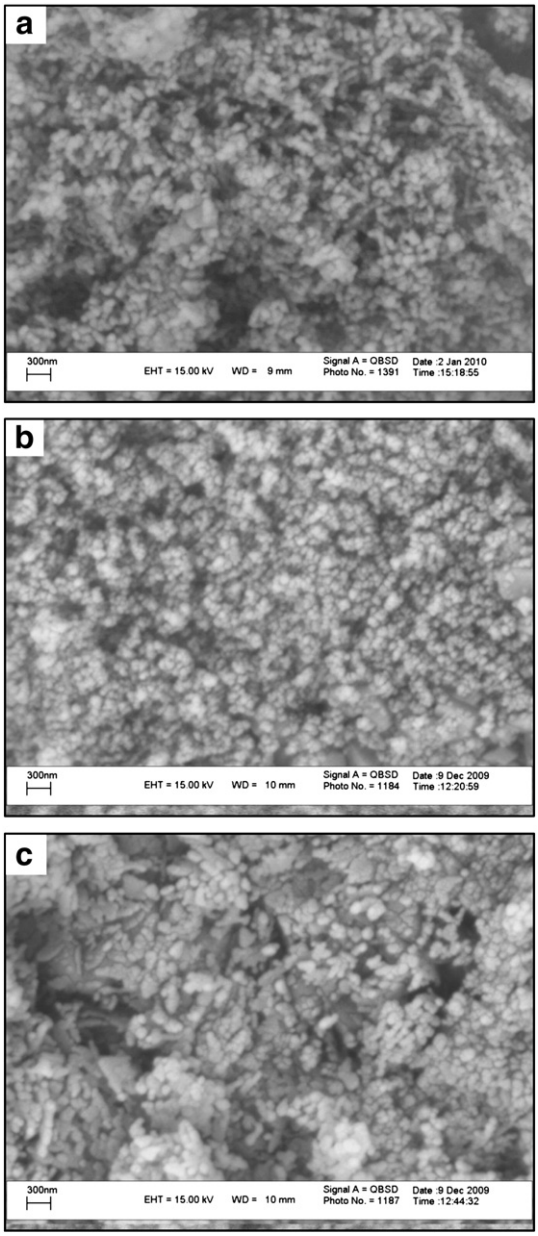

Fig. 6. SEM micrographs of CuO (a), Co_3O_4 (b) and $CuCo_2O_4$ (c) prepared via co-precipitation method.

ions. So the increase of a_0 can be explained by the accommodation of Cu^{2+} at the octahedral sites in the spinel structure [25].

The average crystallite sizes (C.S) of the nanocrystals were calculated using the Debye–Scherer Eq. (2) from the major diffraction peaks.

$$C.S = K.\lambda/\beta.cos\theta. \quad (2)$$

Where K is a constant equal to 0.9, λ is the wavelength of Cu Kα radiation, β is the full width at half maximum (FWHM) of the diffraction peak in radiant and θ is the Bragg angles of the main planes. The average crystallite sizes of CuO, Co_3O_4 and $CuCo_2O_4$ are 16.5, 19.2 and 18.4 nm respectively.

FT-IR spectroscopy is used as a powerful tool to provide supplementary on the nature of metal oxides [47]. Fig. 5 shows comparative FT-IR spectra of CuO, Co_3O_4 and $CuCo_2O_4$. Fig. 5-a shows mid-IR region of these metal oxides, appeared broad bands about 3400 cm^{-1} in all spectra are assigned to both ν_s(O–H) and ν_{as}(O–H) [48], and the less intensive bands at 1632 cm^{-1} are attributed to bending vibration δ(H–O–H) of hydrated water [9]. The region below 1000 cm^{-1} shows intensive band in all spectra which are related to stretching vibration mod of M–O bond and confirm the formation of metal oxide [23,49]. Fig. 5-b shows zoomed region of 400–800 cm^{-1}. FT-IR spectrum of CuO shows abroad band at 525 cm^{-1}. The absorption band of the (Cu^{I}–O) appeared in about 623 cm^{-1} region which was singlet [50,51], but the absorption bands of the (Cu^{II}–O) appeared in about 430–606 cm^{-1} regions which were triplet [39,52]. Hence, the broad band at 525 cm^{-1} can be attributed to the stretching vibrations of (Cu^{II}–O).

After calcining the cobalt citrate–acetate precursor, a soft black powder was obtained which its FT-IR spectrum is shown in Fig. 5-b. The FT-IR spectrum displays two distinct and sharp bands at 580 (ν_1) and 667(ν_2) cm^{-1}, which are attributed to the stretching vibration mode of M–O bond and confirm the formation of Co_3O_4 spinel. The ν_1 band is characteristic of Co^{3+} vibration in the octahedral hole, and ν_2 band is attributable to Co^{2+} vibration in tetrahedral hole in the spinel lattice [23,49,53]. Furthermore, the FT-IR spectrum of $CuCo_2O_4$ reveals two remarkable keen-edge peaks in the range of 800–500 cm^{-1} which are contribution from the spinel phase. The spectrum indicates the presence of two-absorption bands ν_1 at 573 cm^{-1} and ν_2 at 659 cm^{-1}. The band, ν_1, is attributed to the stretching vibration of $Co^{3+}-O^{2-}$ in the tetrahedral complexes and the ν_2 band to that of $Cu^{2+}-O^{2-}$ in the octahedral complexes. The positions of these bands confirm the existence of Cu^{2+} ions entirely in the octahedral sites and the Co^{3+} ions in tetrahedral ones [54,55]. This

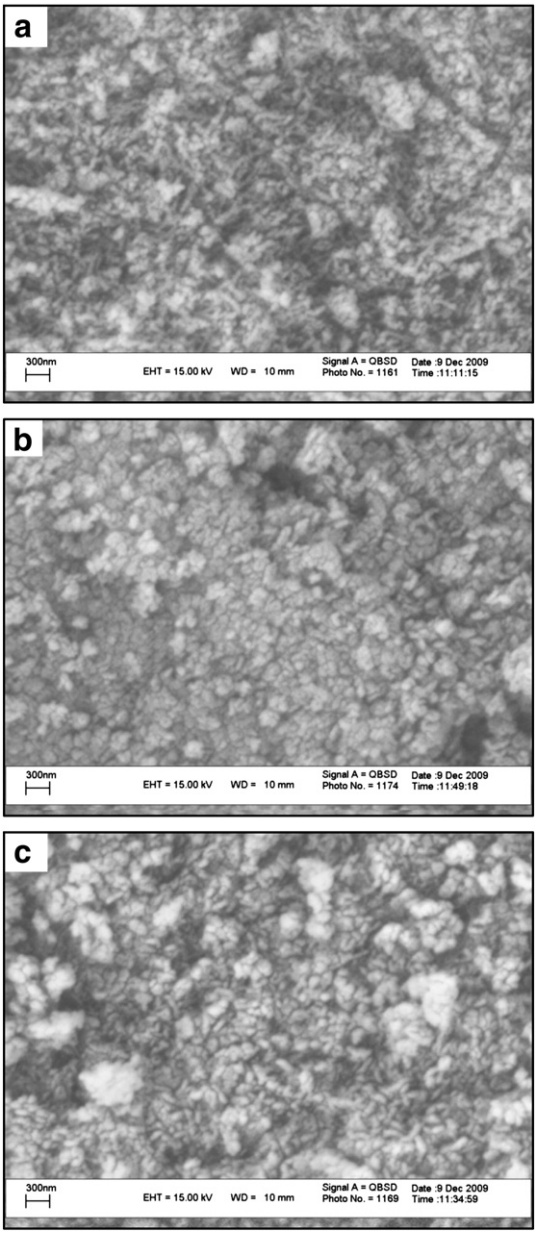

Fig. 7. SEM micrographs of CuO (a), Co_3O_4 (b) and $CuCo_2O_4$ (c) prepared via oxalate decomposition method.

spectroscopic data indicates that $CuCo_2O_4$ is not a mixture of CuO and Co_3O_4 or CuO and Co_2O_3 but a complexity.

Surface morphology of metal oxides was studied by using Scanning Electron Microscopy (SEM). Micrographs of prepared CuO, Co_3O_4 and $CuCo_2O_4$ via co-precipitation method are shown in Fig. 6. The images show that the oxides consist of agglomerated spherical particles with 20–60 nm average particle size whereas the synthesized nano metal oxide powders via oxalate decomposition route consist of strong agglomerated particles with narrow size distribution and no specific shape was observed (Fig. 7). It was noted that the size as well as the nature of the particles somewhat depends upon the temperature and the time of calcination treatment.

The SEM images of synthesized metal oxide via sol–gel route using cetyltrimethylammonium bromide (CTAB) surfactant are shown in Figs. 8–10. The SEM micrographs of CuO are shown in Fig. 8. The SEM images indicate that a large quantity of monodispersed nanorod like CuO with good uniformity was achieved by using this approach. These nanorods have a mean diameter of about 70 nm with little

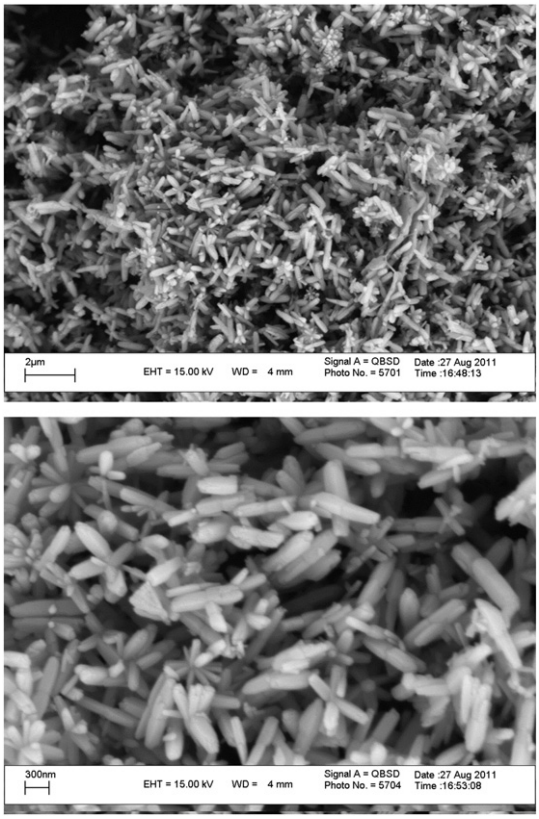

Fig. 8. SEM micrographs of CuO prepared via sol–gel method.

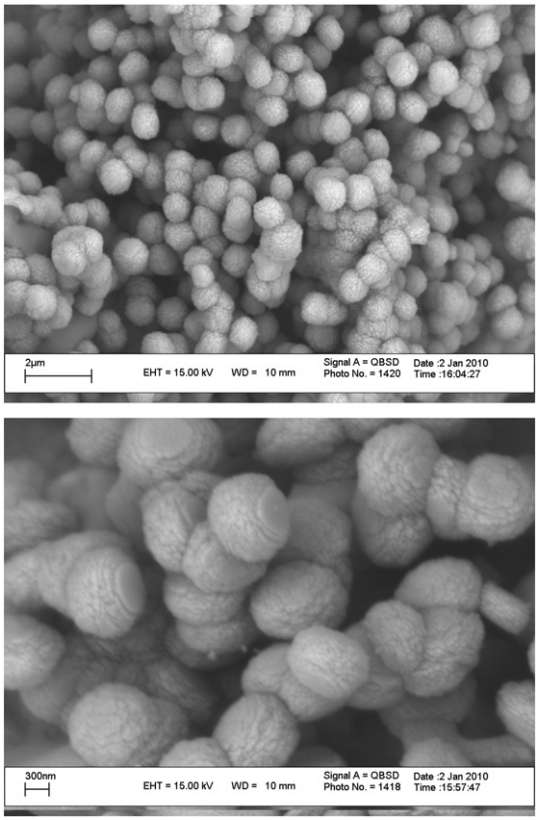

Fig. 9. SEM micrographs of Co_3O_4 prepared via sol–gel method.

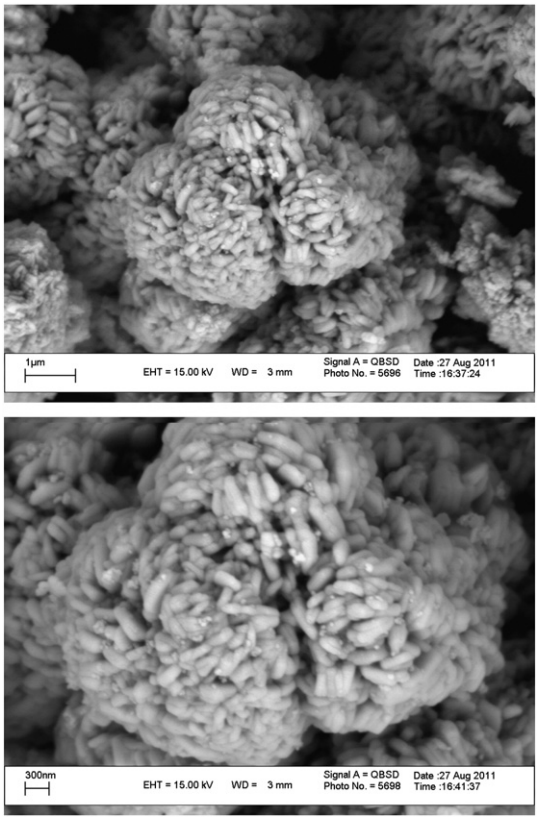

Fig. 10. SEM micrographs of $CuCo_2O_4$ prepared via sol–gel method.

deviation and length of about 200 nm. Fig. 9 shows representative SEM images of the prepared Co_3O_4 samples. Many microparticles, which have uniform and monodisperse similar spherical morphology, are observed. This indicates that our synthesis process definitely is possible for preparation of regular spherical Co_3O_4 nanostructures on a large scale. Typical diameter of the micro-spheres is estimated about 1.1–1.3 μm. The particles are in random arrangement, showing little aggregation. Fig. 10 shows the low and high magnification SEM images of ellipsoid like copper cobaltite with radii between 120 and 200 nm. These images also show that the nanostructure has a cluster formation. In fact, morphology, size, and structure of the final products were controlled using CTAB surfactant. As can be seen the observed morphology of copper cobaltite is incorporation of rod and sphere and it was observed as an ellipsoidal particles.

Table 1 shows the specific surface area, measured by BET method. The results show that all the synthesized powders by sol–gel method are highly dispersive.

Transmission electronic microscopy, TEM, was use to get more information about the shape and crystallite size of synthesized nano powders. Fig. 11 shows the TEM images of synthesized metal oxides via sol–gel method. Typical TEM micrograph of CuO (Fig. 11-a) shows the formation of uniform and monodispersed CuO nanorod with mean diameter and length about 20 and 70 nm, respectively which agrees well with the results that are calculated based on XRD analysis. TEM image of Co_3O_4 in Fig. 11-b shows Co_3O_4 nanoparticles with mean crystallite size about 30–40 nm with strong agglomeration and no specific observable shape. It can be seen that a large number of Co_3O_4 nanocrystals aggregate together and obtained powder are spherical cluster-arranged with diameter of about 300–400 nm. On the other hand, each of the spheres consists of many irregular particles approximately 30–40 nm and the observed morphology is spherical in micrometer scale. TEM image in Fig. 11-c shows that the $CuCo_2O_4$ nanoparticles have a spherical shape with mean size of about 25 nm, which is evident that the particle size agrees well with the crystallite size determined from powder XRD measurements. An individual ellipsoidal nanoparticle with a diameter approaching 200 nm is shown in Fig. 10, which demonstrates that the CuO nanostructures with ellipsoidal shapes are composed of several interconnected sphere-like crystallites with diameter in the range of 18–35 nm.

Table 1
Catalytic activity results of as-synthesized nano-sized metal oxide powders via sol–gel method.

Sample	Catalyst properties		AP thermal decomposition temperature (°C)		
	Crystal size (nm)[a]	Surface area ($m^2\ g^{-1}$)[b]	Phase trans.	First stage	Second stage
Pure AP	–	–	247.24	331.14	443.61
AP + CuO	16.5	61.3	~247	325.72	353.14
AP + Co_3O_4	19.2	56.2	~247	316.14	351.54
AP + $CuCo_2O_4$	18.4	53.4	~247	308.43	340.83

[a] Calculated using the Scherrer's formula on the diffraction peak of maximum intensity.
[b] From BET equation.

3.2. Catalytic activity of oxides

The catalytic behavior of the nano-sized powder on the thermal decomposition of AP was demonstrated by the DSC experiment. The DSC curves of pure AP and the mixtures of metal oxides with AP are shown in Fig. 12. The DSC curve of pure AP indicates its thermal decomposition consists of three stages. In first stage, an endothermic peak is observed at 247.24 °C, which is ascribed to the crystallographic transition of AP from orthorhombic to cubic [56]. In the subsequent two stages, the first exothermic peak appears at 331.14 °C, corresponding to the partial decomposition of AP and formation of an intermediate product and the second, also the main exothermic peak, appears at relatively higher temperature of 443.61 °C, indicating the complete decomposition of the intermediate product into gaseous products [39].

Fig. 12 shows catalytic effect of CuO, Co_3O_4 and $CuCo_2O_4$ on decomposition temperature of AP. DSC endothermic phase transition peaks of AP in presence of any catalysts appeared in the same position around 250 °C, indicating no significant impact of these catalysts on the change of this temperature. However, decomposition stages of AP notably lowered by addition of above-mentioned nano catalysts in compared with pure AP. These temperatures and some other crystal properties of catalysts are listed in Table 1.

According to DSC data, these nano catalysts effectively could be decreased first and second decomposition temperature of AP, also as shown in Table 1, $CuCo_2O_4$ was more effective than others and the thermal decomposition temperature of AP shifts downward about 103 °C.

3.2.1. Mechanism of thermal decomposition of AP

Based on studies in recent years [58–66], two major mechanisms have been proposed for the thermal decomposition of ammonium perchlorate. First: electron transfer from perchlorate ion to ammonium ion, which is as follows:

$$ClO_4^- + NH_4^+ \rightarrow ClO_4^0 + NH_4^0.$$

$$NH_4^0 \rightarrow NH_3 + H.$$

$$ClO_4^0 + ClO_4^- = ClO_4^- + ClO_4^0.$$

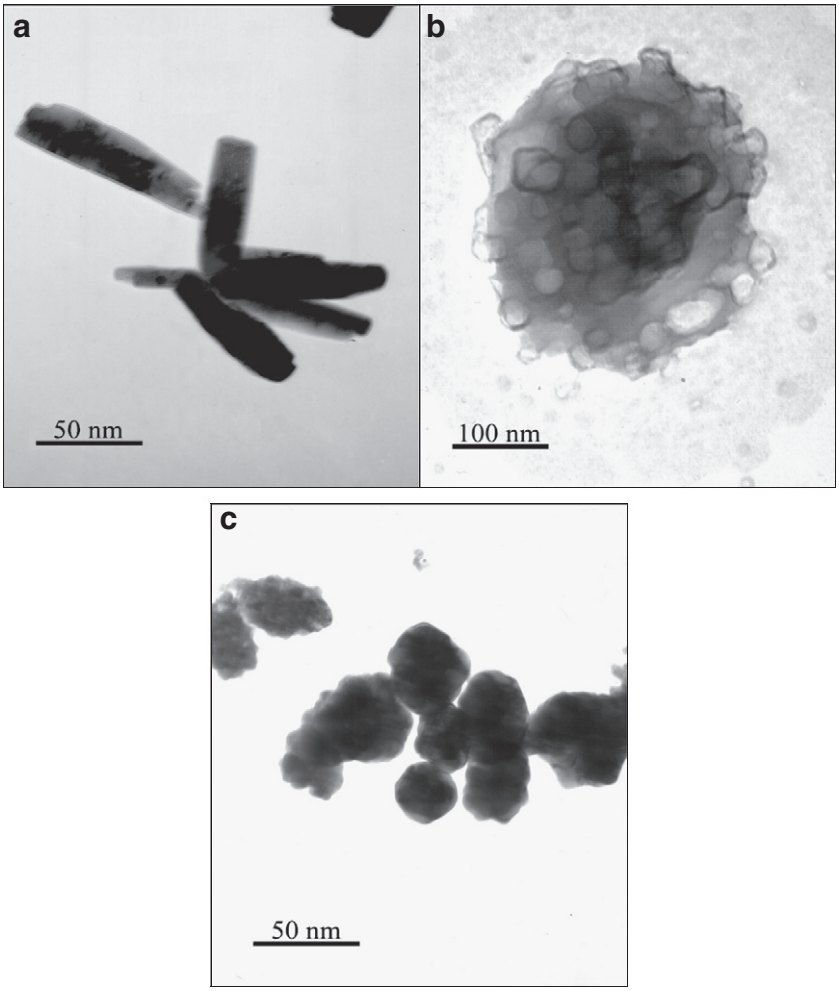

Fig. 11. TEM micrographs of CuO (a), Co_3O_4 (b) and $CuCo_2O_4$ (c) prepared via sol–gel method.

$HClO_4 + H \rightarrow H_2O + ClO_3$.

Second: proton transfer from ammonium ion to perchlorate ion, which is as follows:

$NH_4ClO_{4(s)} \rightarrow NH_4^+ + ClO_4^- \rightarrow NH_{3(s)} + HClO_{4(s)} \rightarrow NH_{3(g)} + HClO_{4(g)}$.

For first mechanism, it is proposed that rate-controlling step is the electron transfer [61,42], and since, CuO, Co_3O_4 and $CuCo_2O_4$ are p-type semiconductor and they have effective sites (positive holes on catalyst surface) for accepting released electron from perchlorate ion. Thus, these catalysts accelerate the electron transfer.

$e^-_{oxide} + ClO_4^- \rightarrow O_{oxide} + ClO_3^- \rightarrow 1/2O_2 + ClO_3^- + e^-_{oxide}$.

Where $e^-{}_{oxide}$ is a positive hole in the valance band of the oxide and O_{oxide} is an abstracted oxygen atom from oxide. It is well known that this mechanism involves two crucial steps: (1) ammonia oxidation and (2) dissociation of ClO_4^- species into ClO_3^- and O_2. In the first step, metal oxides exhibit high and stable catalytic activity toward ammonia oxidation and in the second step metal oxides accept the donated electron from ammonia oxidation, which may promoted the dissociation of ClO_4^- species into ClO_3^- and O_2 [61].

$CuCo_2O_4$ plays better catalytic role than others on AP thermal decomposition. What is reason for that its excellent catalytic role? The presence of a partially filled-3d orbital provides a good explanation of this mechanism. Cu^{2+} and Co^{3+} are all in the presence of a partially filled 3d-orbital. In comparison with single and binary metal oxides, in $CuCo_2O_4$, both Cu^{2+} ($3d^9$) and Co^{3+} ($3d^6$) can easily accept the released electron from ClO_4^- to form stable full-filled 3d-orbital Cu^+ ($3d^{10}$) and Co^{2+} ($3d^7$) cations [59–60].

$Cu^{2+} + ClO_4^- \rightarrow Cu^+ + ClO_4$

$Co^{3+} + ClO_4^- \rightarrow Co^{2+} + ClO_4$.

This is one possible reason that $CuCo_2O_4$ exhibits stronger catalytic activity than probably CuO and Co_3O_4, which shows that $CuCo_2O_4$ has a positive synergistic catalytic effect [59]. In addition, we proposed that the existence of lattice defects in the $CuCo_2O_4$ (Cu^{2+} John–Teller effect) in comparison with Co3O4, probably creates positive holes and electrons. In the decomposition process of AP, $CuCo_2O_4$ provides a bridge for transferred electrons from perchlorate ions to the ammonium ions better than other two metal oxides [62].

For the second mechanism, the primary detected products in the experiments by different researchers were ammonia and perchloric acid [60–64]. This allowed the assumption that the primary stage of AP's thermal decomposition process is proton transfer. This mechanism involves three crucial steps: Step (I) involves a pair of ions in AP lattice. Step (II) involves decomposition or sublimation step that starts with proton transfer from the cation NH_4^+ to the anion ClO_4^-, then the molecular complex is formed and decomposes into NH_3 and $HClO_4$ in Step (III). The molecules of NH_3 and $HClO_4$ either react

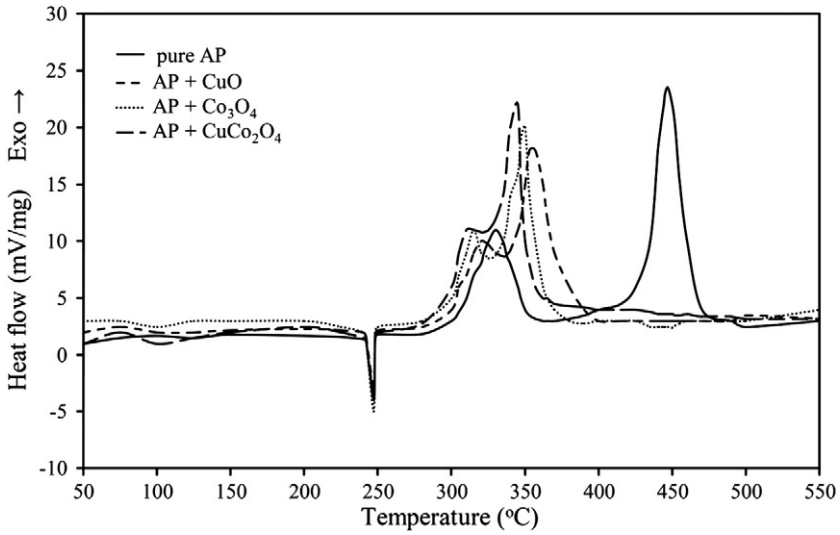

Fig. 12. DSC curves of pure AP and AP with synthesized nano-sized metal oxide powders via sol–gel method.

in the adsorbed layer on the surface of perchlorate or desorbs and sublime interacting in the gas phase [58]:

$$\begin{array}{l} \underset{(I)}{NH_4ClO_4} \leftrightarrow \underset{(II)}{NH_3 - H - ClO_4} \leftrightarrow \underset{(III)}{NH_3 - HClO_4} \\ \qquad\qquad\qquad\qquad\qquad\qquad\qquad\qquad \updownarrow \\ \qquad\qquad\qquad\qquad\qquad\qquad NH_3(a) + HClO_4(a) \\ \qquad\qquad\qquad\qquad\qquad\qquad\quad \updownarrow \qquad\quad \updownarrow \\ \qquad\qquad\qquad\qquad\qquad\qquad NH_3(g) + HClO_4(g). \end{array}$$

In the basis of proton transfer mechanism, during the higher temperature decomposition step, nanoparticles absorb the gaseous reactive molecules on their surface and catalyze the reaction. The creation of more holes within the p-type semiconducting catalysts is responsible for enhancing the decomposition rate of AP. The mechanism of catalytic action is based on the presence of superoxide ion O^{2-} on the surface of catalysts. The O^{2-} species formed during AP's decomposition and the surface O^{2-} species of catalysts are likely the proton traps through the following reaction [39,65]:

$$2NH_4^+ + O^{2-} \rightarrow H_2O + 2NH_3.$$

It is known that the specific surface area, shape and particle size of catalysts are so important factors for proton transfer mechanism and previous studies have shown that by increasing of specific surface area the catalytic efficiency has enhanced. Based on our results, the obtained BET data show that the specific surface areas of synthesized catalysts are approximately equal, and then it seems that the ability of catalysts in O^{2-} creation and gas absorption on their surface, which caused motivation and completion of AP thermal decomposition, is plausible for this reason. $CuCo_2O_4$ in comparison with CuO and Co_3O_4 can produce more O^{2-} species on its surface and accelerate the AP thermal decomposition more than others [66].

As a whole, the catalytic roles that metal oxide additive play in the AP decomposition are still not fully understood.

AP is supposed to have thermal decomposition with chain reaction mechanism as thoroughly scrutinized by YU Zongxue's group [40], and they proposed a mechanism for the decomposition of AP. At low temperature, the products of thermal decomposition of pure AP are NH_3, H_2O and a small amount of N_2O and O_2. During the high-temperature stage of AP's decomposition, HCl, H_2O, N_2O, NH_3, Cl_2, NO, O_2, NO_2 and a small amount of ClO_2 are formed. Based on this mechanism we propose the following route (proton transfer) for the decomposition of AP:

1 At low temperature:

$$NH_4ClO_4 \rightarrow NH_4^+ + ClO_4$$

$$NH_4^+ + ClO_4 \rightarrow NH_3 + HClO_4$$

$$4HClO_4 \rightarrow 2ClO_3 + 2ClO + 3O_2 + 2H_2O$$

$$2NH_3 + 2O_2 \rightarrow N_2O + 3H_2O \leftrightarrow NH_4NO_3 + H_2O.$$

2 At high temperature:

$$4HClO_4 \rightarrow Cl_2 + 5O_2 + 2ClO_2 + 2H_2O$$

$$2Cl_2 + 2H_2O \rightarrow 4HCl + O_2$$

$$2NH_3 + 2ClO_2 \rightarrow N_2O + Cl_2 + 3H_2O$$

$$N_2O + O_2 \rightarrow NO + NO_2.$$

4. Conclusions

In this work, we synthesized nano-sized CuO, Co_3O_4 and $CuCo_2O_4$ powders via different methods including co-precipitation, thermal decomposition of oxalate precursor and sol–gel. Different thermal analysis techniques including TG-DSC and DSC were applied for studying thermal behavior of precursors and some spectroscopic methods such as FT-IR, XRD, SEM and TEM were used for studying structural characteristics of synthesized nano metal oxides. Interpretation of obtained results from XRD, SEM and TEM studies certified the formation of nano sized particles of these oxides. The catalytic activities of as-synthesized metal oxides on thermal decomposition of AP were tested. $CuCo_2O_4$ showed better catalytic activity than others and shifted the AP thermal decomposition temperature downwardly to about 103 °C. Two mechanisms based on proton and electron transfer processes have also been proposed for AP decomposition in the presence of nano-sized powder oxides.

Acknowledgments

Financial supports from the Islamic Azad University, Ardabil Branch and Tabriz University are gratefully acknowledged. The

authors are highly thankful to Dr. Ahmad Bagheri and Mohammad Reza Nourani for taking TEM images.

References

[1] T.R. Hinklin, J. Azurdia, M. Kim, J.C. Marchal, S. Kumar, R.M. Laine, Finding spinel in all the wrong places, Advanced Materials 20 (2008) 1373–1375.

[2] T.J. Yoon, J.S. Kim, B.G. Kim, K.N. Yu, M.H. Cho, J.K. Lee, Multifunctional nanoparticles possessing a "Magnetic Motor Effect" for drug or gene delivery, Angewandte Chemie International Edition 44 (2005) 1068–1071.

[3] J.F. Marco, J.R. Gancedo, M. Gracia, J.L. Gautier, E.I. Ríos, H.M. Palmer, C. Greaves, F. J. Berry, Cation distribution and magnetic structure of the ferrimagnetic spinel $NiCo_2O_4$, Journal of Materials Chemistry 11 (2001) 3087–3309.

[4] R. Xu, H.C. Zeng, Self-generation of tiered surfactant superstructures for one-pot synthesis of Co_3O_4 nanocubes and their close and non-close-packed organizations, Langmuir 20 (2004) 9780–9790.

[5] C. Sol, R.J.D. Tilley, Ultraviolet laser irradiation induced chemical reactions of some metal oxides, Journal of Materials Chemistry 11 (2001) 815–820.

[6] S.H. Hong, J.S. Bae, H.J. Ahn, Synthesis of nano-sized Co_3O_4 powder by spray conversion method for anode material of lithium battery, Metals and Materials International 14 (2) (2008) 229–232.

[7] M. Ando, T. Kobayashi, S. Iijima, M. Haruta, Optical recognition of CO and H_2 by use of gas-sensitive Au–Co_3O_4 composite films, Journal of Materials Chemistry 7 (1997) 1779–1783.

[8] P. Nkeng, J.F. Koenig, J.L. Gautier, P. Chartier, G. Poillerat, Enhancement of surface areas of Co_3O_4 and $NiCo_2O_4$ electrocatalysts prepared by spray pyrolysis, Journal of Electroanalytical Chemistry 402 (1996) 81–89.

[9] M. Verelst, T.O. Ely, C. Amiens, E. Snoeck, P. Lecante, A. Mosset, M. Respaud, J.M. Broto, B. Chaudret, Synthesis and characterization of CoO, Co_3O_4 and mixed Co/CoO nanoparticules, Chemistry of Materials 11 (1999) 2702–2708.

[10] D. Barreca, C. Massignan, S. Daolio, M. Fabrizio, C. Piccirillo, L. Armelao, E. Tondello, Composition and microstructure of cobalt oxide thin films obtained from a novel cobalt(II) precursor by chemical vapor deposition, Chemistry of Materials 13 (2001) 588–593.

[11] M. Gotic, I.C. Nagy, S. Popovic, S. Music, Formation of nanocrystalline $NiFe_2O_4$, Philosophical Magazine Letters 78 (1998) 193–201.

[12] A. Chatterjee, D. Das, S.K. Pradhan, D. Chakravorty, Synthesis of nanocrystalline nickel–zinc ferrite by the sol–gel method, Journal of Magnetism and Magnetic Materials 127 (1993) 214–218.

[13] M. Hamdani, J.F. Koenig, P. Chartier, Films minces de Co_3O_4 et $NiCo_2O_4$ obtenus par nébulisation réactive (spray) pour l'électrocatalyse. II. Etude par voltampérométrie cyclique, Journal of Applied Electrochemistry 18 (1988) 568–576.

[14] A.A. Athawale, M. Bapat, A soft solution process to synthesize nanocrystalline barium zirconate via reactive solid state precursors, Journal of Metastable and Nanocrystalline Materials 23 (2005) 3–6.

[15] M.Y. Li, W.S. Dong, C.L. Liu, Z. Liu, F.Q. Lin, Ionic liquid-assisted synthesis of copper oxalate nanowires and their conversion to copper oxide nanowires, Journal of Crystal Growth 310 (2008) 4628–4634.

[16] Y. Liu, X. Zhang, Effect of calcination temperature on the morphology and electrochemical properties of Co_3O_4 for lithium-ion battery, Electrochimica Acta 54 (2009) 4180–4185.

[17] P.R. Arya, P. Jha, A.K. Ganguli, Synthesis, characterization and dielectric properties of nanometer-sized barium strontium titanates prepared by the polymeric citrate precursor method, Journal of Materials Chemistry 13 (2003) 415–423.

[18] A.K. Ganguli, T. Ahmad, P.R. Arya, P. Jha, Nanoparticles of complex metal oxides synthesized using the reverse-micellar and polymeric precursor routes, Pramana, Journal of Physics 65 (2005) 937–947.

[19] M. Boutonnet, J. Kizling, P. Stenius, G. Maire, The preparation of monodisperse colloidal metal particles from microemulsions, Colloids and Surfaces 5 (1982) 209.

[20] J. Zhu, Q. Gao, Mesoporous MCo_2O_4 (M═Cu, Mn and Ni) spinels: Structural replication, characterization and catalytic application in CO oxidation, Microporous and Mesoporous Materials. 124 (2009) 144–152.

[21] T. Ozkaya, A. Baykal, M.S. Toprak, Y. Koseoğlu, Z. Durmuş, Reflux synthesis of Co_3O_4 nanoparticles and its magnetic characterization, Journal of Magnetism and Magnetic Materials 321 (2009) 2145–2149.

[22] F. Svegl, B. Orel, I. Grabec-Svegl, V. Kaucic, Characterization of spinel Co_3O_4 and Li-doped Co_3O_4 thin film electrocatalysts prepared by the sol–gel route, Electrochimica Acta 45 (2000) 4359–4371.

[23] M. Salavati-Niasari, N. Mir, F. Davar, Synthesis and characterization of Co_3O_4 nanorods by thermal decomposition of cobalt oxalate, Journal of Physics and Chemistry of Solids 70 (2009) 847–852.

[24] S. Angelov, E. Zhecheva, K. Petrov, D. Menandjiev, The properties of a spinel copper cobaltite prepared at low temperatures and normal pressure, Materials Research Bulletin 17 (1982) 235–240.

[25] B. Chi, H. Lin, J. Li, Cations distribution of $Cu_xCo_{3-x}O_4$ and its electro catalytic activities for oxygen evolution reaction, International Journal of Hydrogen Energy 33 (2008) 4763–4768.

[26] M.D. Koninck, S.C. Poirier, B. Marsan, $Cu_xCo_{3-x}O_4$ used as bifunctional electrocatalyst. Electrochemical characterization for the oxygen reduction reaction, Journal of the Electrochemical Society 154A (2007) 381–388.

[27] A.L. Rosa-Toro, R. Berenguer, C. Quijada, F. Montilla, E. Morallón, J.L. Vázquez, Preparation and characterization of copper-doped cobalt oxide electrodes, The Journal of Physical Chemistry. B 110 (2006) 24021–24029.

[28] N. Fradette, B. Marsan, Surface studies of $Cu_xCo_{3-x}O_4$ electrodes for the electrocatalysis of oxygen evolution, Journal of the Electrochemical Society 145 (1998) 2320–2327.

[29] R. Bonchev, T. Zheleva, S.C. Sevov, Morphological and compositional characterization of copper–cobalt spinel made by mechanochemical reactions, Chemistry of Materials 2 (1990) 93–95.

[30] A. Sugier, E. Freund, *Process for manufacturing alcohols, particularly linear saturated primary alcohols, from synthesis gas*, US patent (1978) 4,122,110.

[31] Y. Sharma, N. Sharma, G.V. Subba Rao, B.V.R. Chowdari, Nanophase $ZnCo_2O_4$ as a high performance anode material for Li-ion batteries, Advanced Functional Materials 17 (2007) 2855–2861.

[32] T. Baird, K.C. Campbell, P.J. Holliman, R.W. Hoyle, M. Huxam, D. Stirling, B.P. Williams, M. Morris, Cobalt–zinc oxide absorbents for low temperature gas desulfurization, Journal of Materials Chemistry 9 (1999) 599–605.

[33] G.Z. Gassan–zedeh, S.F. Seyidbayova, The heterogeneous catalytic reduction of NO and N_2O mixture by carbon monoxide, Applied Catalysis B: Environmental 42 (2003) 359–367.

[34] B. Cui, H. Lin, J.B. Li, X. Li, J. Yang, J. Tao, Core–ring structured $NiCo_2O_4$ nanoplatelets: synthesis, characterization, and electrocatalytic applications, Advanced Functional Materials 18 (2008) 1440–1472.

[35] J.F. Marco, J.R. Gancedo, M. Gracia, J.L. Gautier, E. Ríos, F.J. Berry, Characterization of the nickel cobaltite, $NiCo_2O_4$, prepared by several methods: an XRD, XANES, EXAFS, and XPS study, Journal of Solid State Chemistry 153 (2000) 74–81.

[36] P. Boldrin, A.K. Hebb, A.A. Chaudhry, L. Otley, B. Thiebaut, P. Bishop, J.A. Darr, Direct synthesis of nanosized $NiCo_2O_4$ spinel and related compounds via continuous hydrothermal synthesis methods, Industrial and Engineering Chemistry Research 46 (2007) 4830–4838.

[37] G. Fortunato, H.R. Oswald, A. Reller, Spinel-type oxide catalysts for low temperature CO oxidation generated by use of an ultrasonic aerosol pyrolysis process, Journal of Materials Chemistry 11 (2001) 905–911.

[38] W. Wei, W. Chen, D.G. Ivey, Rock salt-spinel structural transformation in anodically electrodeposited Mn–Co–O nanocrystals, Chemistry of Materials 20 (2008) 1941–1947.

[39] L. Chen, L. Li, G. Li, Synthesis of CuO nanorods and their catalytic activity in the thermal decomposition of ammonium perchlorate, Journal of Alloys and Compounds 464 (2008) 532–536.

[40] Z. Yu, L. Chen, L. Lu, X. Yang, X. Wang, DSC/TG-MS study on in situ catalytic thermal decomposition of ammonium perchlorate over CoC_2O_4, Chinese Journal of Catalysis 30 (1) (2009) 19–23.

[41] S.G. Christoskova, M. Stoyanova, M. Georgieva, D. Mehandjiev, Preparation and characterization of a higher cobalt oxide, Materials Chemistry and Physics 60 (1999) 39–43.

[42] H. Liu, Q. Jiao, Y. Zhao, H. Li, Ch. Sun, X. Li, Mixed oxides derived from Cu–Co layered double hydroxide nanorods: preparation, characterization and their catalytic activities, Journal of Alloys and Compounds 496 (2010) 317–323.

[43] D.V. Survase, M. Gupta, S.N. Asthana, The effect of Nd_2O_3 on thermal and ballistic properties of ammonium perchlorate (AP) based composite propellants, Progress in Crystal Growth and Characterization of Materials 45 (2002) 161–165.

[44] A.A. Said, R. Al-Qasmi, The role of copper cobaltite spinel, $Cu_xCo_{3-x}O_4$ during the thermal decomposition of ammonium perchlorate, Thermochimica Acta 275 (1) (1996) 83–91.

[45] A. Tang, H. Yang, X. Zhang, Mechanochemical route to synthesize Co_3O_4/CuO composite nanopowders, International Journal of the Physical Sciences 1 (2) (2006) 101–105.

[46] J. Zhou, X. Shen, M. Jing, Nanosized Ni–Mn oxides prepared by the citrate gel process and performances for electrochemical capacitors, Journal of Materials Science and Technology 22 (2006) 803–806.

[47] C.A. Melendres, G.A. Bowmaker, J.M. Leger, B. Beden, In-situ synchrotron far infrared spectroscopy of surface films on a copper electrode in aqueous solutions, Journal of Electroanalytical Chemistry 449 (1998) 215–218.

[48] I. Luisetto, F. Pepe, E. Bemporad, Preparation and characterization of nano cobalt oxide, Journal of Nanoparticle Research 10 (2008) 59–67.

[49] M.A. Gabal, A.A. El-Bellihi, S.S. Ata-Allah, Effect of calcination temperature on Co(II) oxalate dehydrate-iron(II) oxalate dihydrate mixture: DTA–TG, XRD, Mössbauer, FT-IR and SEM studies, Materials Chemistry and Physics 81 (2003) 8492.

[50] C. Ehrhardt, M. Gjikaj, W. Brockner, Thermal decomposition of cobalt nitrato compounds: preparation of anhydrous cobalt (II) nitrate and its characterisation by Infrared and Raman spectra, Thermochimica Acta 432 (2005) 36–40.

[51] Y.R. Uhm, J.H. Park, W.W. Kim, M.K. Lee, C.K. Rhee, Novel synthesis of Cu_2O nano cubes derived from hydrolysis of Cu nano powder and its high catalytic effects, Materials Science and Engineering A 449 (2007) 817–820.

[52] A. Jagminas, G. Niaura, J. Kuzmarskyt, R. Butkien, Surface-enhanced Raman scattering effect for copper oxygenous compounds array within the alumina template pores synthesized by ac deposition from Cu(II) acetate solution, Applied Surface Science 225 (2004) 302–308.

[53] Y. Chen, Y. Zhang, S. Fu, Synthesis and characterization of Co_3O_4 hollow spheres, Materials Letters 61 (2007) 701–705.

[54] J.P. Singh, R.N. Singh, New active spinel-type $M_xCo_{3-x}O_4$ films for electroanalysis of oxygen evolution, Journal of New Materials for Electrochemical Systems 3 (2000) 131–139.

[55] R.N. Singh, T. Sharma, A. Singh, Anindita, D. Mishra, Electrocatalytic activities of nano-sized spinel-type $Cu_xCo_{3-x}O_4$ ($0 \le x \le 1$) for methanol oxidation in alkaline solutions, International Journal of Electrochemical Science 2 (2007) 762–777.

[56] F. Solymosi, E. Krix, Catalysis of solid phase reactions effect of doping of cupric oxide catalyst on the thermal decomposition and explosion of ammonium perchlorate, Journal of Catalysis 1 (1962) 468–480.

[57] B. Chi, H. Lin, J. Li, N. Wang, J. Yang, Comparison of three preparation methods of $NiCo_2O_4$ electrodes, International Journal of Hydrogen Energy 31 (2006) 1210–1214.
[58] Sh. Zhao, D. Ma, Preparation of $CoFe_2O_4$ nanocrystallites by solvothermal process and its catalytic activity on the thermal decomposition of ammonium perchlorate, Journal of Nanomaterials 2010 (2010) 5.
[59] Y. Wang, X. Xia, J. Zhu, Y. Li, X. Wang, X. Hu, Catalytic activity of nanometer-sized CuO/Fe_2O_3 on thermal decomposition of AP and combustion of AP-based propellant, Combustion Science and Technology 183 (2011) 154–162.
[60] G. Singh, I.P.S. Kapoor, Sh. Dubey1, P.F. Siril, Preparation, characterization and catalytic activity of transition metal oxide nanocrystals, Journal of Scientific Conference Proceedings 1 (2009) 11–17.
[61] Sh. Chaturvedi, P.N. Dave, Nano-metal oxide: potential catalyst on thermal decomposition of ammonium perchlorate, Journal of Experimental Nanoscience (2011) 1–27.
[62] T. Liu, L. Wang, P. Yang, B. Hu, Preparation of nanometer $CuFe_2O_4$ by auto-combustion and its catalytic activity on the thermal decomposition of ammonium perchlorate, Materials Letters 62 (2008) 4056–4058.
[63] H. Xu, X. Wang, L. Zhang, Selective preparation of nanorods and micro-octahedrons of Fe_2O_3 and their catalytic performances for thermal decomposition of ammonium perchlorate, Powder Technology 185 (2008) 176–180.
[64] S.S. Josh, P.R. Patil1, V.N. Krishnamurthy, Thermal decomposition of ammonium perchlorate in the presence of nanosized Ferric Oxide, Defence Science Journal 58 (2008) 721–727.
[65] L. Li, X. Sun, X. Qiu, J. Xu, G. Li, Nature of catalytic activities of CoO nanocrystals in thermal decomposition of ammonium perchlorate, Inorganic Chemistry 47 (2008) 8839–8846.
[66] M.D. Koninck, S. Poirier, B. Marsan, $Cu_xCo_{3-x}O_4$ used as bifunctional electrocatalyst: physicochemical properties and electrochemical characterization for the oxygen evolution, Journal of the Electrochemical Society 153 (2006) A2103–A2110.